THE GEOLOGICAL SOCIETY OF AMERICA®

# Path and amount of dextral fault slip in the Eastern California shear zone across the central Mojave Desert

**Joseph E. Andrew† and J. Douglas Walker**
*Department of Geology, University of Kansas, Lawrence, Kansas 66045, USA*

## ABSTRACT

**New total fault slip estimates for the central Mojave Desert portion of the Eastern California shear zone support through-going dextral shear of ~18 km that is transferred northward to the Garlock fault. The Eastern California shear zone accommodates ~25% of the plate-boundary shear, with the transversely oriented Garlock fault forming its northern boundary with the Walker Lane belt. Total fault slip estimates for the major faults in the central Mojave Desert were determined using detailed geologic mapping supplemented with aeromagnetic data. Offset data for the Blackwater fault show a consistent 1.8 ± 0.1 km of dextral slip along 55 km of strike length, and they indicate that slip initiated at or after 3.8 Ma. The faults adjacent to the Blackwater fault have dextral slip of: 4.8 ± 0.3 km (Harper Lake fault); 2.9 ± 0.5 km (Mount General fault); 1.0 ± 0.7 km (Lockhart fault); and 3.2 ± 0.3 and 0.53 ± 0.05 km (Paradise fault). These slip data augment published data for the central Mojave Desert and allow evaluation of the strain path in the central Mojave Desert, showing consistent along-strike, through-going dextral slip. Contractional and extensional step-overs in the central Mojave Desert accommodate a change from focused slip in the southern central Mojave Desert to a wider and more dispersed fault system northward with a shift in the locus of dextral shear westward. We interpret these changes in the fault system to be a response to the Garlock fault, which inhibits through-going faulting but allows through-going dextral shear via clockwise deflection of its trace.**

## INTRODUCTION

The area east of the San Andreas transform in California accommodates 25% of the active dextral shear between the Pacific and North American plates (Dixon et al., 1995; Miller et al., 2001; Bird, 2009). Dextral shear in this region is focused on two distinct zones of faulting, the Eastern California shear zone and the Walker Lane belt, separated by the transversely oriented, sinistral Garlock fault (Fig. 1). Numerous geologic and geodetic studies have examined the regional and local aspects of the fault slip in this region as a way to understand the lithospheric controls on this plate-margin deformation zone. Faults in the Walker Lane belt (sensu Stewart, 1988) north of the Garlock fault have well-known kinematics and slip histories (Andrew and Walker, 2009). The total offset of faults in the Eastern California shear zone south of the Garlock fault is only partially well known, and the timing of initiation of these structures is poorly known (Glazner et al., 2002; Oskin et al., 2007). The incomplete fault slip data set for the Eastern California shear zone limits our understanding of how dextral shear is accommodated across the Garlock fault in the combined Eastern California shear zone–Garlock fault–Walker Lane belt system.

The Eastern California shear zone accommodates active dextral shear across a 120-km-wide zone (Dokka and Travis, 1990). The western portion of the Eastern California shear zone, the central Mojave Desert, has numerous structures that show Holocene or late Pleistocene activity (Amoroso and Miller, 2006; Miller et al., 2007, 2013) but few constraints on slip amounts. The dextral Blackwater-Calico fault system (Fig. 1) is the best-studied through-going structure within the central Mojave Desert. The slip on this system decreases from 9.6 km on the Calico fault in the south (Fig. 1; Dibblee, 1967; Glazner et al., 2000; Oskin et al., 2007), to 3.0 km in the Calico Hills (Singleton and Gans, 2008), to 1.8 km at Black Mountain (Oskin and Iriondo, 2004), and a northern termination of offset was interpreted to occur ~7 km south of the Garlock fault (Smith, 1964; Oskin and Iriondo, 2004).

The lack of data constraining slip amounts for faults in the Eastern California shear zone near the Garlock fault permits multiple hypotheses for how regional deformation is accommodated, such as: (1) dextral slip dies out northward into off-fault strain in the numerous east-west–trending folds within the central Mojave Desert (Dibblee, 1967; Oskin et al., 2007); (2) strain is transferred rightward via east-west–striking sinistral-oblique or normal faults to the northeastern Mojave Desert (Schermer et al., 1996; Miller et al., 2001; Meade and Hager, 2004; Oskin et al., 2007); or (3) deformation is transferred leftward via east-west–trending contractional step-over structures (Bartley et al., 1990; Glazner and Bartley, 1994). Regardless of the exact path that strain takes through the central Mojave Desert, the Garlock fault appears to be a barrier to through-going, northwest-striking dextral faults, so regional dextral strain across it needs to be taken up via significant clockwise deflection of the Garlock fault trace (Fig. 1; Garfunkel, 1974; Dokka and Travis, 1990; Gan et al., 2003) or transferred around the eastern end of the Garlock fault. More information about slip on faults in the central Mojave Desert is required to evaluate these hypotheses.

This study examined several faults in the northern part of the central Mojave Desert to test the hypotheses for the strain path in the Eastern California shear zone. Oskin et al. (2007) and Frankel et al. (2008) noted that changes in dextral slip along the Blackwater-Calico fault system occur near locations of active north-south contraction (Glazner and Bartley, 1994) and intersections with transverse left-lateral and extensional faults. Impetus for the current study came from data in Andrew et al. (2014), which demonstrate that ~2 km of dextral slip on the northern end of the Blackwater fault occurs to within 3 km of the Garlock fault, thus negating at least part of the interpretation that slip decreases northward for the Blackwater-Calico fault system. To collect a full slip budget in the central Mojave Desert, our study examined dextral fault slip in the region using the Calico fault as the eastern boundary of the southern central Mojave Desert; northward, we used either the Paradise fault or the east Goldstone Lake fault (domain boundary of the northeast Mojave Desert as defined by Schermer et al. [1996]) and

†jeandrew@ku.edu

 doi: 10.1130/B31527.1; 7 figures; 2 tables.

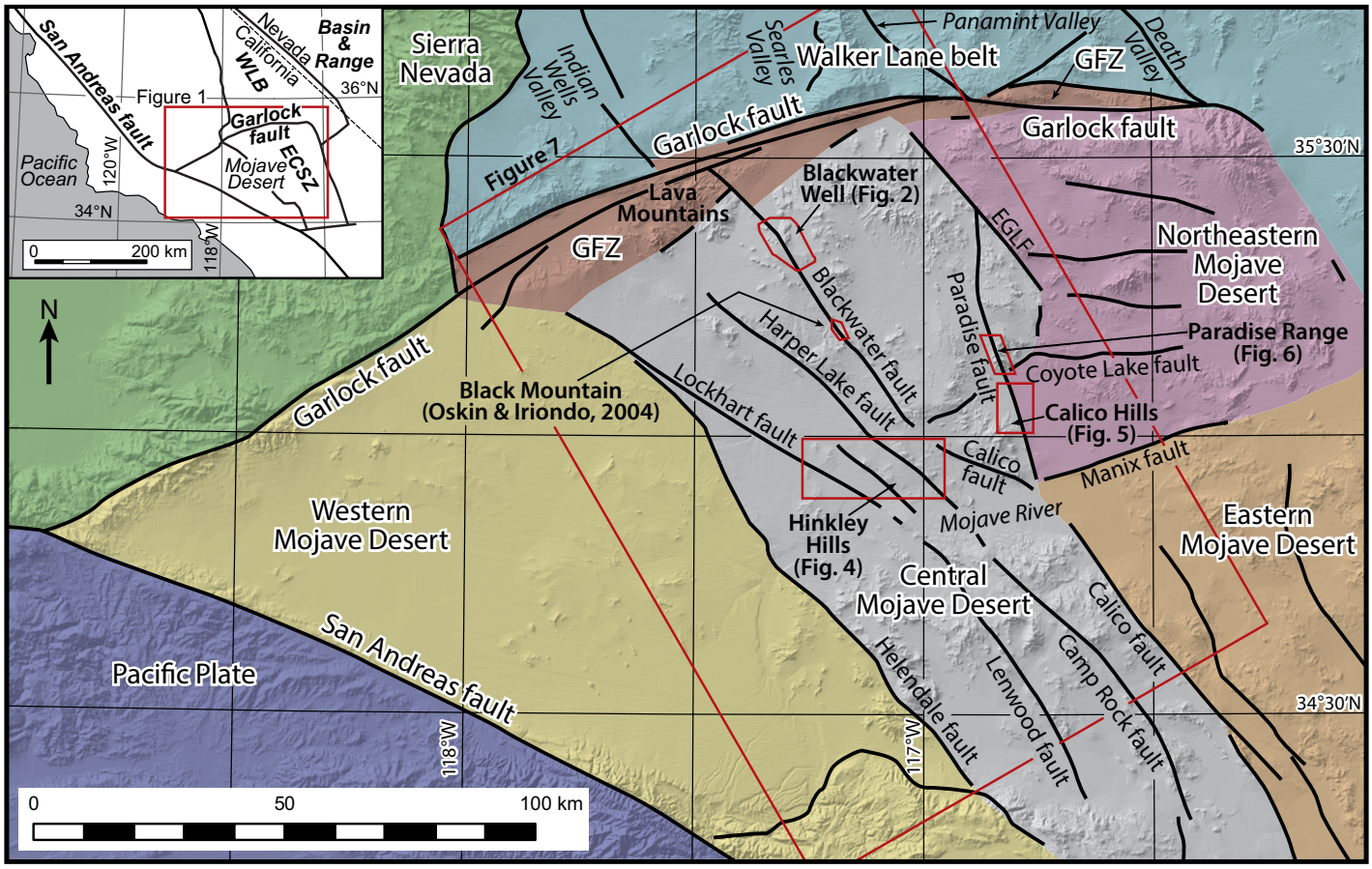


**Figure 1. Shaded relief map of the Eastern California shear zone showing deformation provinces. See inset map for location. Faults are modified from the Southern California Community Fault Model (Plesch et al., 2007) and Quaternary fault maps of Amoroso and Miller (2006) and Miller et al. (2013). The Garlock fault is a 10–20-km-wide fault zone (Garlock fault zone [GFZ]) where it borders the Eastern California shear zone (ECSZ) and Walker Lane belt (WLB; Andrew et al., 2014). EGLF—east Goldstone Lake fault.**

Miller and Yount [2002]). Note that two recent large ($M$ >7) earthquakes in the Eastern California shear zone (1992 Landers and 1999 Hector Mine earthquakes) have occurred on faults near the southeastern boundary of the central Mojave Desert.

We investigated geologic units and structures to examine fault slip at new sites along the Blackwater fault and then compared these with fault offset data of Oskin and Iriondo (2004) and Andrew et al. (2014) to better understand how total slip varies along the length of the fault (i.e., to differentiate consistent, gradually decreasing, or incrementally decreasing slip). Next, we examined new slip constraints along the Harper Lake, Mount General, Lockhart, and Paradise faults, adjacent to the Blackwater fault (Fig. 1). Last, we combined these data with published total offset data in the central Mojave Desert to examine the fault slip in this system, and specifically the roles of off-fault strain, transfer of strain northward, and lateral step-over structures.

## FAULT SLIP ESTIMATES FOR THE BLACKWATER FAULT

The southern portion of the Blackwater fault (Fig. 1) has 1.8 ± 0.1 km of dextral offset of a ca. 3.8 Ma basalt lava flow near Black Mountain (Oskin and Iriondo, 2004). (Note, uncertainties on fault slip reported here, and by most authors, are usually near the extremes of possible values, so we assume they represent 2σ or 95% confidence estimates.) Dextral slip at the northern end of the Blackwater fault is ~2 km based on two fault slip marker sets: 2.1 ± 0.6 and 1.9 ± 0.3 km (Andrew et al., 2014). Our study examined a site on the central portion of the Blackwater fault to determine how slip varies along strike.

### Geology of the Central Blackwater Fault

The Blackwater fault near Blackwater Well (Fig. 1) has fault line scarps (Fig. 2) that cut 7.2 Ma dacite lava flows (Oskin and Iriondo, 2004), and on remote-sensing images, it shows right-lateral separation of distinct Mesozoic plutonic units with steeply dipping contacts (see Table 1 for rock descriptions). Oskin and Iriondo (2004) concluded that dextral slip on the Blackwater fault in this area is between 0.3–1.8 km, based on reconstructions of these lava flows, assuming minimal erosion since ca. 7 Ma. The minimal erosion assumption is difficult to support because the base of these flows is exposed on a mesa ~120 m above the surrounding terrain (Fig. 2). Quaternary fault maps (Amoroso and Miller, 2006; Miller et al., 2007, 2013) show that at least one additional fault splay of the Blackwater fault occurs west of the dacite lava flow, outside the study area of Oskin and Iriondo (2004).

The late Miocene dacite lava flow is exposed on the east side of the Blackwater fault (Fig. 2). It was deposited directly onto biotite granodiorite, but locally there are paleochannels cut into the granodiorite with three varieties of paleochannel fill: an older pumice lapilli tuff deposit; an overlying pebble sandstone containing grano-

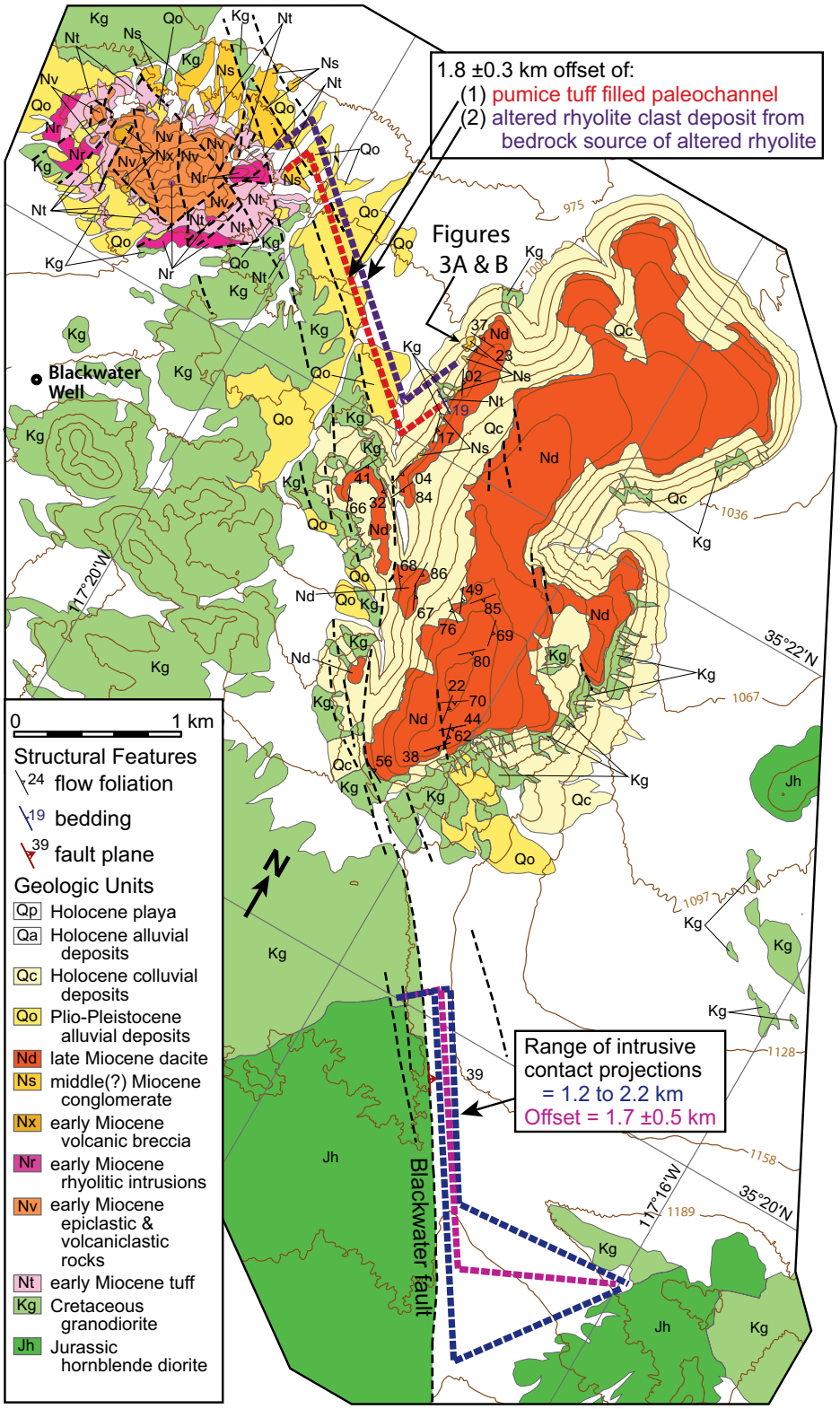


**Figure 2. Geologic map of central segment of the Blackwater fault near Blackwater Well (mapped at 1:6000 scale, using methods outlined in Andrew et al., 2014). See Figure 1 for location. See Table 1 for detailed descriptions of geologic units. This map includes geologic mapping data of an early Miocene rhyolite center (Jenkins, 1989) north of Blackwater Well and of a late Miocene dacite lava east of Blackwater Well (Oskin and Iriondo, 2004). Thick dashed lines are projections of fault offset geologic markers; see labels and text for details.**

diorite, aplite, and unaltered rhyolite clasts; and a boulder conglomerate of altered rhyolite clasts (see Table 1 for descriptions). The altered rhyolite clasts occur distinctly as boulders up to 4 m in diameter (Figs. 3A and 3B) that are yellow colored, silicified, and flow banded.

An early Miocene rhyolitic volcanic center occurs west of the Blackwater fault, north of Blackwater Well (Figs. 2 and 3C). This is a relatively small-volume center dominated by rhyolitic lapilli and lithic lapilli tuffs (see Table 1 for descriptions) with overlying proximal epiclastic and volcaniclastic units of unaltered rhyolite lava that are intruded by strongly altered, flow-banded rhyolitic bodies (Jenkins, 1989). Erosion of the rhyolitic volcanic center has created distinctive alluvial deposits that vary radially; locations with rhyolitic intrusions upslope have distinctive fanglomerate deposits with yellow boulders of silicified and flow-banded rhyolite. These subrounded to subangular boulders are 0.7–2.0 m in diameter, with some up to 4 m across. Several fault scarps and fault-line scarps of the Blackwater fault cut the inactive alluvial deposits that were shed northeastward from this rhyolitic volcanic center.

## Fault Slip Interpretation for the Central Blackwater Fault

We interpreted several fault slip markers for the Blackwater fault using our new data. We estimated the horizontal component of fault slip because the Blackwater fault is dominantly a right-lateral strike-slip fault (Oskin and Iriondo, 2004). A steeply dipping intrusive contact of light-colored Cretaceous granodiorite into chloritized Jurassic hornblende diorite occurs on both sides of the Blackwater fault (Fig. 2). This contact strikes northeast, where it is well exposed west of the Blackwater fault. East of the Blackwater fault, the contact is buried by alluvium adjacent to the fault but is exposed 1.2 km farther eastward. We estimated the trend of the map trace of the intrusive contact in order to project it westward to the fault. We tried to account for the variability of the exposed map trace by estimating the extreme angles of possible projections to the Blackwater fault (where the estimated extreme angles of projection limit the possible dextral slip from 1.2 to 2.2 km). These projections yield a fault slip estimate of 1.7 ± 0.5 km (this includes the dextral offset on the small splay faults just west of the main fault trace; Fig. 2).

Rock types in the rhyolitic volcanic center match the composition of clasts in paleochannels below the dacite lava east of the Blackwater fault. The boulders of altered, yellow-colored, silicified, and flow-banded rhyolite in the paleochannel fill deposits (Figs. 3A and 3B) match

TABLE 1. DESCRIPTIONS OF NEOGENE GEOLOGIC UNITS IN THE BLACKWATER WELL AREA

| Unit descriptions for units on Figure 2 | Side* |
|---|---|
| Late Miocene dacite lava | |
| A 7.23 ± 1.07 Ma dacite lava flow (Oskin and Iriondo, 2004) that is a 60–90-m-thick, dark-colored, vitrophyric dacite with abundant fine-grained needles of hornblende. It has strong flow textures with an oxidized basal autobreccia zone up to 6 m thick, overlain by flow-banded lava with platy fractures grading upward into massive lava capped by a carapace of autobreccia (Fig. 3A). | East |
| Middle(?) Miocene conglomerate | |
| Paleochannel fill deposits below dacite lava flow consisting of weakly indurated pebble sandstone to boulder conglomerate. Bedding is locally well exposed where the unit is finer grained. Clasts consist of biotite granodiorite; aplite; unaltered, massive, gray rhyolite lava; and yellow-altered, silicified, flow-banded rhyolite lava. The granodiorite and aplite clasts match the immediately underlying basement rocks, but the rhyolite clasts have no known source in the area east of the Blackwater fault. The clast size varies for each composition: Granodiorite and aplite clasts are up to 25 cm in diameter, the unaltered rhyolite clasts are up to 1 m, and the silicified rhyolite lava clasts are generally coarser, up to 4 m in diameter. Altered and unaltered rhyolite clasts do not occur in the same paleochannel deposits. The abundance, size, and rock type of clasts in the paleochannel deposits vary along base of the dacite lava, with northeastern exposures containing the coarsest altered rhyolite clasts (Figs. 2, 3A, and 3B). Arkosic pebble sandstone and conglomerate in the southern paleochannel deposit overlie pumice lapilli tuff. | East |
| Early Miocene volcanic breccia | |
| Local deposits of poorly sorted volcanic clasts, including unaltered massive rhyolite lava. The clasts size ranges from sand-sized to 3 m boulders. The chaotic sorting, coarse clast size, and unbedded nature suggest these are proximal talus breccias (Jenkins, 1989). | West |
| Early Miocene rhyolitic intrusions | |
| Altered, flow-banded rhyolitic bodies intruded into the rhyolitic volcanic center. There are several of these intrusions in the volcanic center, but only one intrusion is exposed adjacent to the Blackwater fault (Figs. 2 and 3C). Strong alteration is centered on the intrusions, with abundant pyrite mineralization and intense silicification grading outward to moderate to low argillitization (Jenkins, 1989). This mineralization has been subsequently altered by supergene processes replacing pyrite with jarosite, creating rocks with a distinctive bright yellow color. We interpret these rhyolitic intrusions to be part of a regional early Miocene volcanic episode (early Miocene volcanism summarized in Glazner et al., 2002). | West |
| Early Miocene epiclastic and volcaniclastic rocks | |
| Proximal epiclastic and volcaniclastic deposits of thinly laminated lithic siltstones and thick beds of massive breccia with interbeds of ash-fall lithic and lapilli tuffs. The matrix consists of ash particles. Boulder-sized clasts of unaltered, gray rhyolite lava occur up to 1.5 m in diameter. | West |
| Early Miocene tuff | |
| Basal volcanic deposits of felsic lithic and lapilli tuffs in the volcanic center west of the Blackwater fault. These tuffs range from thin beds (1 mm) to thick massive beds (3 m). The units contain varying amounts of lithic and pumice fragments in a tuffaceous matrix. One sub-dacite paleochannel on the east side of the Blackwater fault contains a deposit of massive pumice lapilli tuff. It is very light gray to white, containing abundant unaltered, rhyolitic pumice lithic clasts. This tuff is 4 m thick and fills a northeast-trending paleovalley. | Both |
| Cretaceous granodiorite | |
| Biotite granodiorite forms the basement rocks of the northern parts of the area. It is a medium-grained, equigranular, leucocratic biotite granodiorite that contains steeply dipping, 10–20-cm-thick aplite dikes and shallowly dipping, 1–2-m-thick pegmatitic dikes. This granodiorite intrudes hornblende diorite. | Both |
| Jurassic hornblende diorite | |
| The basement rock exposed in the southern parts of the map area is chloritized hornblende diorite. This unit is medium to coarse grained and has a dark green color due to the prevalence of chlorite alteration. Series of shallowly dipping, 1–2-m-thick pegmatite dikes also cut this diorite. | Both |

*Refers to side of the Blackwater fault on which these units are exposed.

jarosite-altered, silicified, flow-banded rhyolitic intrusive bodies in the rhyolitic volcanic center immediately west of the Blackwater fault. The paleochannel boulders of altered rhyolite have similar shapes, textures, and sizes as clasts in sedimentary deposits sourced from the rhyolitic intrusions in the rhyolitic volcanic center. The geologic relationships at the rhyolitic volcanic center, with its eastern end of dominantly rhyolitic tuff beds and small volumes of volcaniclastic breccia of unaltered rhyolite lava, limit the source area for the yellow, altered rhyolite clasts to one altered rhyolitic intrusion on the eastern side of the volcanic center adjacent to the Blackwater fault (Fig. 2). The pumice lapilli tuff in the paleochannel below the dacite lava, east of the Blackwater fault, matches texturally and lithologically with a tuff exposed just west of the Blackwater fault along the eastern side of the rhyolitic center (Fig. 2). The volcanic rocks west of the Blackwater fault that occur adjacent to the Blackwater fault have a northwest to southeast variation in rock type: a core of altered rhyolitic intrusive rocks surrounded to the north and south by pumice lapilli tuff deposits and capped with volcaniclastic deposits of unaltered rhyolite lava clasts. The spacing of this variation in the geology for the volcanic center is similar to that seen in paleochannels east of the Blackwater fault below the ca. 7 Ma dacite lava. A fault slip constraint can be constructed by matching projections of these multiple units to the Blackwater fault (Fig. 2) to yield 1.8 ± 0.3 km of dextral slip. This slip estimate is based on the orientation of the northeast-trending paleochannel filled by pumice lapilli tuff and includes the range of possible horizontal projection azimuths of this channel westward to the fault. This slip value is compatible within error with the right-lateral offset interpreted for the nearby intrusive contact of granodiorite into diorite discussed earlier. Jachens et al. (2002) estimated a similar amount of dextral offset (2.0 km) for a linear aeromagnetic high in an area just a few kilometers north of our study area.

## Regional Fault Slip for the Blackwater Fault

The new offset data for the central Blackwater fault demonstrate the continuous nature of slip along much of the length of the Blackwater fault. These values, combined with published geologic offsets to the north and south of Blackwater Well by Oskin and Iriondo (2004) and Andrew et al. (2014), show that ~1.8 km of right-lateral slip occurs along 55 km of the trace of the Blackwater fault (Table 2). Because these values are consistent, slip cannot significantly diminish going northward along the fault as interpreted by Oskin and Iriondo (2004).

The ages of geologic features that have ~1.8 km of dextral offset on the Blackwater fault vary from Pliocene (Oskin and Iriondo, 2004) to Cretaceous, with several offset late Miocene features in the Lava Mountains (Andrew et al., 2014) and at Blackwater Well (Oskin and Iriondo, 2004). These features are scattered along the length of the fault, and all have the same amount of offset within error. We interpret this to imply that significant dextral slip on this fault began at or after ca. 3.8 Ma, which is the age of the youngest known geologic unit with the full 1.8 km of dextral offset. Oskin and Iriondo (2004) interpreted slip to have begun before 3.8 Ma based on interpretation of a basaltic lava flow filling a paleochannel along the fault trace, but the context of this paleotopographic

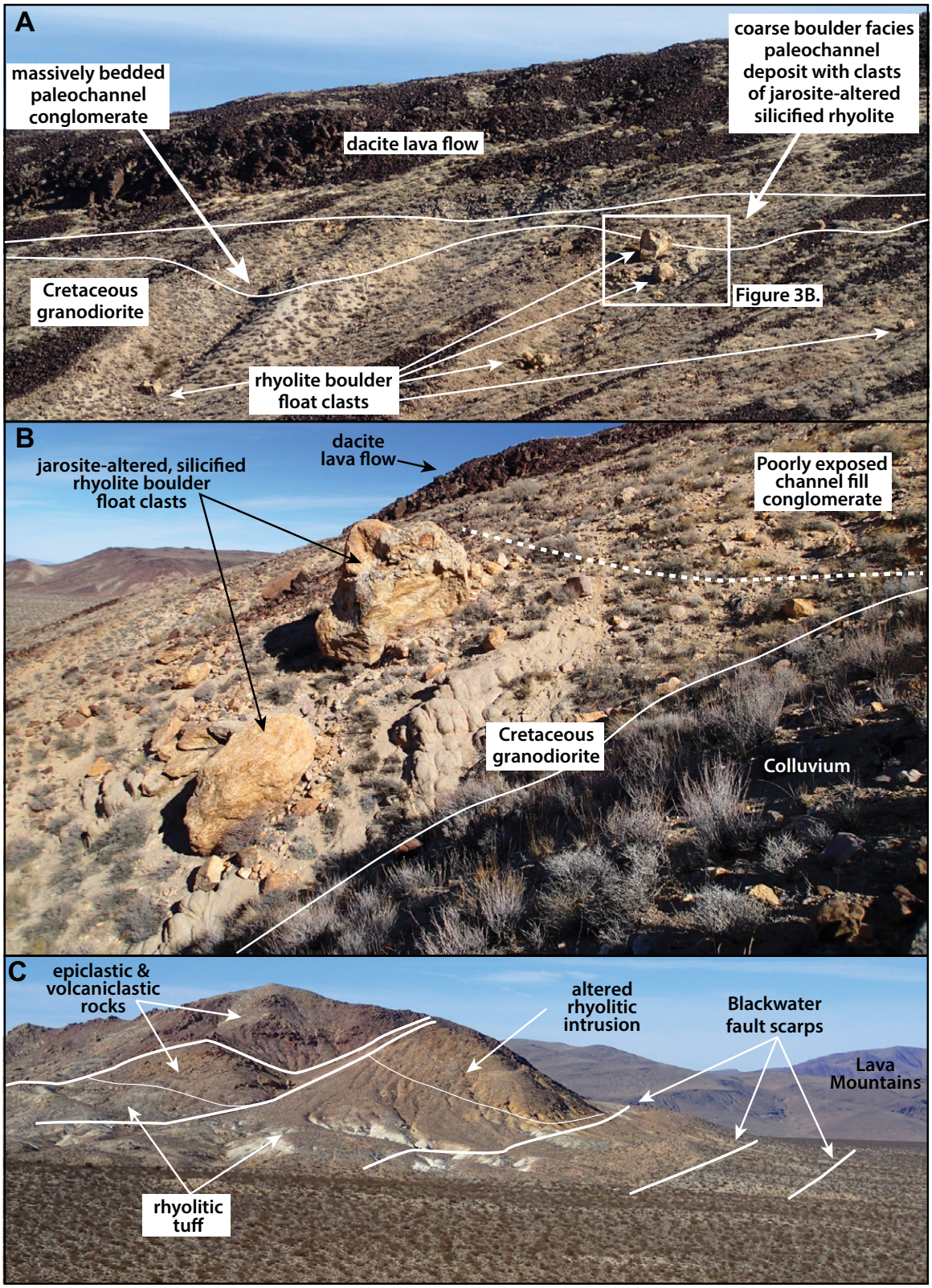


**Figure 3. (A) View of a paleochannel deposit below a 7.2 Ma dacite lava flow. See Figure 2 for location. This deposit contains coarse boulder clasts of jarosite-altered silicified rhyolite lava. Scale varies, but the largest boulder to the right of center is 4 m high. (B) Detailed view of A, showing jarosite-altered silicified rhyolite lava boulders that have moved a few meters downslope from the paleochannel deposit. The largest boulder in this view is 4 m tall. (C) View looking west to the early Miocene rhyolitic center, north of Blackwater Well, as shown on Figure 2. Hill in middle ground is approximately 150 m high. Geologic data are annotated on this view with thicker lines as faults and fault-line scarps.**

TABLE 2. HORIZONTAL COMPONENT OF TOTAL DEXTRAL FAULT SLIP IN THE CENTRAL MOJAVE DESERT

| Label* | Offset features and notes | Offset (km) | Error (±km) | Reference |
|---|---|---|---|---|
| Blackwater fault | | | | |
| B1 | Distal and proximal facies of Almond Mountain Volcanics (7.5–8.0 Ma) | 2.1 | 0.6 | Andrew et al. (2014) |
| B2 | Buttress unconformity of Bedrock Spring Formation (7–10 Ma) onto older dacite domes of the volcanics of the Summit Range (10.5–11.5 Ma) | 1.9 | 0.3 | Andrew et al. (2014) |
| B3 | Jarosite-altered, silicified rhyolite clasts under 7.2 Ma dacite lavas (Oskin and Iriondo, 2004) to sedimentary source area of altered rhyolite lava (Fig. 2) | 1.8 | 0.3 | This study |
| B4 | Intrusive contact of granodiorite into hornblende diorite (Fig. 2) | 1.7 | 0.5 | This study |
| B5 | Lava flow edges of Pliocene basalt flows | 1.8 | 0.1 | Oskin and Iriondo (2004) |
| B | Weighted mean of offsets for Blackwater fault | 1.81 | 0.09 | This study |
| Calico fault | | | | |
| C1 | Langtry-Waterloo silver-barite hydrothermal deposit | 2.6 | 0.7 | Fletcher (1986) |
| C2 | Celadonite-altered dacite domes in Calico Mountains | 3.0 | 0.1 | Singleton and Gans (2008) |
| C | Weighted mean of C1 and C2 | 2.99 | 0.10 | This study |
| Calico folds | | | | |
| CF | Interpreted shortening of the Pickhandle Formation | 1.0 | 0.3 | Singleton and Gans (2008) |
| Camp Rock fault | | | | |
| SC | 7.56 km of offset of Miocene-age Silver Bell fault plus 0.98 km on a splay fault and 1.24 km from adjacent drag folding | 9.78 | 0.14 | Glazner et al. (2000) |
| Camp Rock fault | | | | |
| CR1 | As the Camp Rock fault approaches the Lenwood anticline, its strike changes from 325° to 290°, and slip diminishes to zero | 0 | N.D. | Gurney (2008) |
| CR2 | Fault contact of interbedded volcanic-sedimentary rock with steeply dipping tuff overlying gneiss, diorite, and granite | 1.6 | N.D. | Hawkins (1976) |
| CR3 | Granite-quartz monzonite contact. Full offset: CR1 and CR2 have less slip due to accommodation on the Lenwood anticline | 3.75 | N.D. | Miller and Morton (1980) |
| East Goldstone Lake fault | | | | |
| EG | Correlation of intrusive contacts between Cretaceous muscovite-garnet granite and Jurassic quartz diorite | 3 | N.D. | Schermer et al. (1996) |
| Gravel Hills fault | | | | |
| GH | Interpreted additional 1.2 km of dextral slip transferred to the northern Harper Lake fault from the Calico fault via the Black Mountain anticline | 6.0 | 0.3 | This study |
| Harper Lake fault | | | | |
| HL | Aggregate of intrusive contact, fold hinges, and folded detachment fault and rock units (for more details, see Fig. 4 and text) | 4.8 | 0.3 | This study |
| Helendale fault | | | | |
| H | Reevaluation of 3 km offset of distinctive plutons by Miller and Morton (1980) using digitally relocated data of Dibblee (1960c) onto detailed orthophotographs | 3.2 | 0.2 | Miller and Morton (1980); This study |
| Lenwood anticline | | | | |
| LA1 | Eastern: subtract Camp Rock fault slip from west Lenwood fold | 1.1 | N.D. | Gurney (2008) |
| LA2 | Western: modeled contraction from fault-bend fold model | 3.8 | N.D. | Gurney (2008) |
| Lenwood fault | | | | |
| LW | Distinctive 7.33 Ma (Iriondo, *cited in* Frankel et al., 2008), xenolith-bearing basalt flows in Fry Mountains | 1.0 | 0.2 | Carleton (1988) |
| Lockhart fault | | | | |
| LK | Aggregate of intrusive contact, fold hinges, and folded detachment fault and rock units (for more details, see Fig. 4 and text). | 1.0 | 0.7 | This study |
| Mount General fault | | | | |
| MG | Aggregate of intrusive contact, fold hinges, and folded detachment fault and rock units (for more details, see Fig. 4 and text) | 2.9 | 0.5 | This study |
| Paradise fault | | | | |
| P1 | Aeromagnetic pattern that corresponds to magnetic highs of Mesozoic plutonic rocks and lows of Paleozoic metasedimentary rocks (Fig. 5) | 3.1 | 0.3 | This study |
| P2 | Paleozoic quartzite intruded by Mesozoic plutons (McCulloh, 1960; Dudash, 2006), relocated to detailed orthophotographs (Fig. 5) | 3.4 | 0.5 | This study |
| PS | Weighted mean of P1 and P2 | 3.18 | 0.26 | This study |
| PN | Weighted mean of four offsets of Mesozoic plutonic rocks on Figure 6 reinterpreted from McCulloh (1960) using detailed orthophotographs | 0.53 | 0.05 | This study |

*Labels on Figure 7; not all of these are shown on Figure 7.

low is unknown. This channel may be coincidental, or it may represent pre–3.8 Ma faulting with dextral slip amounts smaller than our measurement errors, or it may represent an earlier episode of dip slip (earlier sinistral slip is ruled out because of the similar amounts of dextral slip of Pliocene to Cretaceous features).

We computed the reduced $\chi^2$ values (often referred to as mean standard weighted deviation [MSWD] by geoscientists) for the slip estimates for the Blackwater fault because there are five estimates for slip. The reduced $\chi^2$ value for these data is 0.39 ($P = 0.18$), with a weighted average slip of 1.81 ± 0.09 km (2σ). The relatively low reduced $\chi^2$ value indicates that the slip uncertainties on this fault may be overestimated in our analysis and in other studies.

## FAULT SLIP ESTIMATES FOR OTHER CENTRAL MOJAVE DESERT FAULTS

The total dextral slip for the other major faults in the central Mojave Desert adjacent to the Blackwater fault is poorly known. The Harper Lake, Mount General, Lockhart, and Paradise faults (Fig. 1) are well-mapped features with pronounced geomorphic expression (Dibblee,

1967; Amoroso and Miller, 2006; Miller et al., 2007, 2013). Estimates of the total slip values of these faults are necessary if we are to evaluate fault slip through the central Mojave Desert. Our analysis of these faults uses published geologic data supplemented with aeromagnetic data sets summarized in Jachens et al. (2002), which were published electronically by the U.S. Geological Survey. Jachens et al. (2002) used these aeromagnetic data sets to estimate 28 fault slip values across the Eastern California shear zone, a few of which are mentioned herein where applicable.

Bartley et al. (1992) examined features of an early Miocene extensional complex in the Hinkley Hills area to estimate dextral slip for the Harper Lake and Mount General faults (Fig. 1) of 3–4 km and 5–10 km, respectively. The Hinkley Hills area has a Jurassic gneissic to mylonitic mafic plutonic complex that is juxtaposed with Paleozoic and Proterozoic metasedimentary biotite schist (Fig. 4A). Mesoscale folding along northeast-trending axes is responsible for repetition of these units. These rocks are intruded by the early Miocene Waterman Hills granite (Bartley et al., 1992; Glazner et al., 1994; Fletcher et al., 1995; Walker et al., 1995). Early Miocene bedrock is well exposed along the east sides of the Mount General and Harper Lake faults (Fig. 4A), but there is extensive Quaternary alluvial cover along their west sides and along the Lockhart fault. This poor exposure of bedrock limits the precision of slip estimates because it requires more inference and projection of contacts.

The mesoscopic folds have northeast-trending, shallow-plunging fold axes with steeply dipping limbs (Fletcher et al., 1995; Walker et al., 1995). The folding occurred in the early Miocene before initiation of dextral faulting

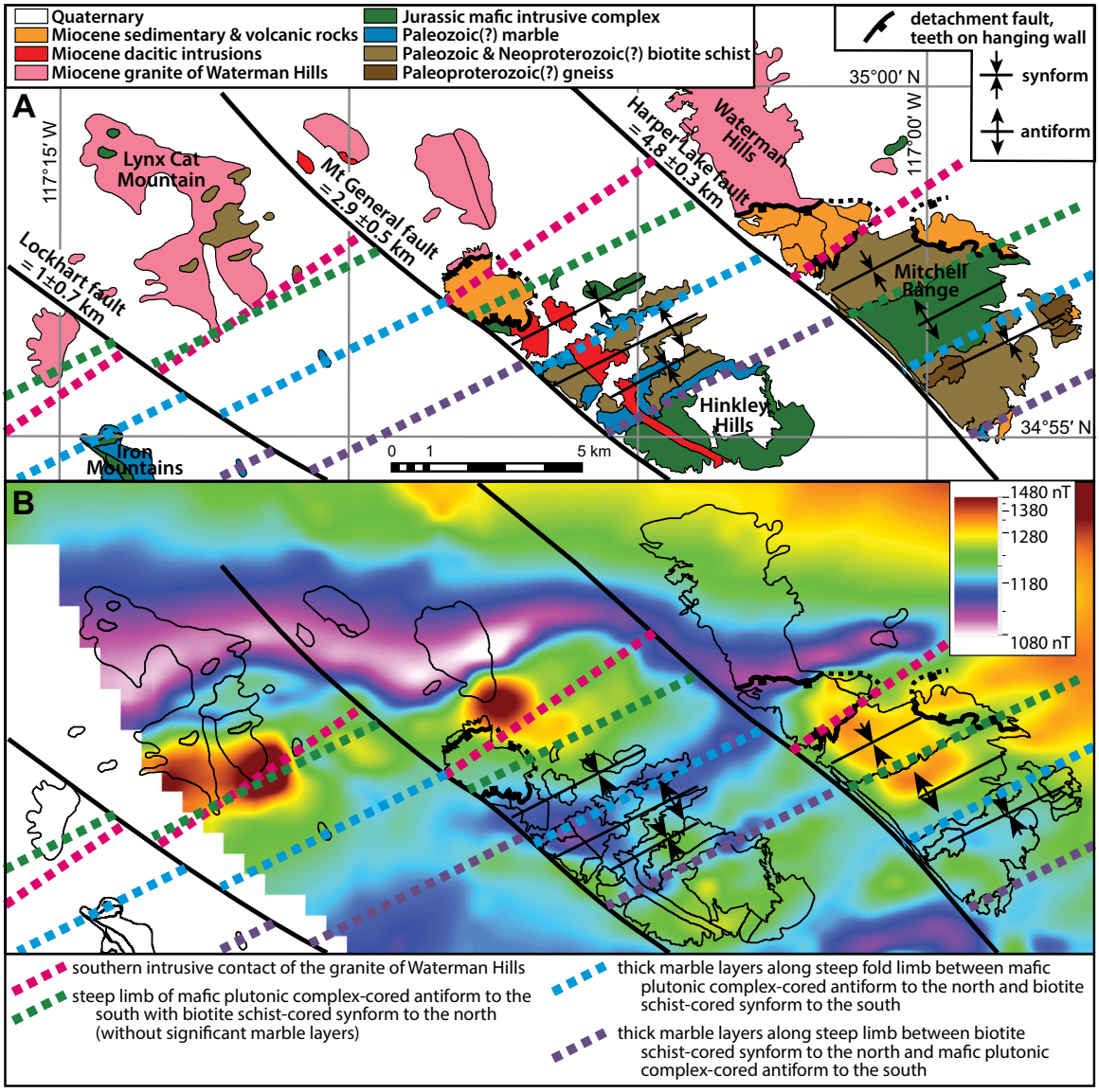


**Figure 4. (A) Geologic map of the Hinkley Hills area with simplified and locally inferred geologic markers shown by thick dashed lines. See Figure 1 for location. Data are modified from Dibblee (1960b), Fletcher et al. (1995), Fletcher and Martin (1998), and Walker et al. (2002). (B) Detailed aeromagnetic data (electronically published digital data from the U.S. Geological Survey compiled in Jachens et al., 2002) overlain by geologic map features and markers in the same area as part A. These aeromagnetic data represent multiple data sets that have been adjusted to an arbitrary datum.**

in the Eastern California shear zone (Glazner et al., 2002). The folds create a systematic outcrop pattern oriented perpendicular to the dextral faults. The granite of the Waterman Hills intrudes these folded rocks with a steep contact that is oblique to the trend of the fold hinges (Fletcher et al., 1995; Fletcher and Martin, 1998; Fletcher, 1999). An early Miocene detachment fault is exposed in the Mitchell Range and in Hinkley Hills (Fig. 4A). This contact is folded, and outcrops of it and its upper plate of early Miocene volcanic rocks occur in the hinges of mesoscopic synclines/synforms. The presence of the shallowly dipping detachment fault on both sides of the Harper Lake fault supports an assumption of similar levels of exposure.

None of the individual bedrock markers in the Hinkley Hills area is unambiguous or well enough exposed to be used as a piercing point, but a composite of several of these features does create a pattern that can be matched across the Harper Lake fault (Fig. 4A). These features include: the intrusive contact of the Miocene Waterman Hills granite; the folded detachment fault; mafic igneous complex rocks; and thick, steeply dipping marble beds in the biotite schist. The intrusive contact of the Waterman Hills granite is poorly exposed, but it creates a consistent pattern of aeromagnetic highs and lows (Fig. 4B). An aeromagnetic high is associated with the intrusive contact of this granite, but the interior is a magnetic low. The aeromagnetically defined granite contact is offset dextrally along the Harper Lake and Mount General faults.

Our analysis used detailed, digital geologic mapping data for the Hinkley Hills, Mitchel Range–Waterman Hills, and Iron Mountains (Fig. 4; Boettcher, 1990; Boettcher and Walker, 1993; Fletcher et al., 1995; Fletcher and Martin, 1998; Fletcher, 1999; Walker et al., 2002), supplemented with older mapping data from Dibblee (1960a, 1960b) and Walker et al. (1990), which were all replotted and relocated onto 1-m-resolution digital orthophotographs. Restoration of dextral fault slip (horizontal component) of the aggregate features yields fault slip estimates of 4.8 ± 0.3 km for the Harper Lake fault, 2.9 ± 0.5 km for the Mount General fault, and 1.0 ± 0.7 km for the Lockhart fault. The precision of this restoration is poor across the Mount General and Lockhart faults because not all features are present in the intervening fault block. We estimated the extremes of map-based geometric projection errors for these faults based on the variability of the trends of these traces and the distance of projections to the faults. These slip values are similar to those estimated by Jachens et al. (2002) using aeromagnetic data for the Mount General and Harper Lake faults of 3.1 and 5.0 km, respectively.

The Paradise fault was recently recognized as a major neotectonic fault with a suggested offset of at least a few hundred meters (Fig. 1; Miller and Yount, 2002; Miller et al., 2007, 2013). We estimated slip on the southern parts of the Paradise fault from offset features in the eastern Calico Hills. McCulloh (1960) mapped a northeast-striking body of Paleozoic metasedimentary rocks that were intruded by Jurassic mafic plutonic rocks and overlain and intruded by early Miocene rocks (Fig. 5A). The eastern part of the Paleozoic rocks is covered by Quaternary deposits near the trace of the Paradise fault (Dudash, 2006). Another sequence of Paleozoic metasedimentary rocks occurs on the east side of the Paradise fault a few kilometers to the south. Correlation of these metasedimentary rocks implies 3.4 ± 0.5 km of dextral slip on the Paradise fault (Table 2). Similar dextral offset is observed in the aeromagnetic data (Fig. 5B), which show 3.1 ± 0.3 km of dextral offset of the south edge of an aeromagnetic high (offset marker drawn at the inflection of the slope in the aeromagnetic data) just north of the Paleozoic rocks. The magnetic low in Figure 5B correlates with the Paleozoic metasedimentary rocks, and the high to the north is due to Jurassic plutonic rocks that intrude the Paleozoic rocks. The offset estimate using the Paleozoic rock map data is somewhat higher because they are exposed farther away from the fault on the west side and require a greater amount of projection to the Paradise fault trace. A weighted mean of these slip estimates for the Paradise fault is 3.2 ± 0.3 km (Table 2).

The trace of the Paradise fault continues northward past the intersection with the Coyote Lake fault and into the Paradise Range (Fig. 1). We reinterpreted geologic map data of McCulloh (1960) using high-resolution remote-sensing images (Fig. 6A) for offset on the newly recognized Paradise fault. The Paradise fault is easily seen in the remote-sensing images (Fig. 6A) where it cuts numerous steeply dipping plutonic contacts of Mesozoic units in this area of the fault trace. Four of these reinterpreted intrusive contacts were used to measure offset along the Paradise fault (Fig. 6B) and yielded a weighted mean of 0.53 ± 0.05 km of dextral offset (Table 2). The surficial and geologic map of Miller et al. (2013) shows a plutonic contact in this same area with a similar value of 0.5 km of dextral offset. Aeromagnetic data support this interpretation of ~0.5 km of dextral offset. Additional possible dextral faulting may occur in the alluvial valley west of the Paradise Range (Fig. 6A), but aeromagnetic and geologic data of McCulloh (1960) limit that offset to <1 km of dextral offset.

## TOTAL FAULT SLIP IN THE CENTRAL MOJAVE DESERT

The known total offsets along dextral faults and interpreted shortening accommodated by Neogene folds in the central Mojave Desert are summarized in Figure 7 and Table 2. We computed weighted means of slip estimates for faults in the central Mojave Desert for which we had multiple estimates of slip (Table 2), e.g., the Blackwater, north Calico, and Paradise faults. Important sources of uncertainty to area-wide interpretations include the limited offset data for the northernmost portions of the central Mojave Desert, with the exception of the Blackwater fault.

The Helendale fault is the westernmost fault in our central Mojave Desert analysis. Miller and Morton (1980) estimated slip of the Helendale to be 3 km based on mapping of the intrusive contact between distinctive Mesozoic plutons (located at H on Fig. 7). We reevaluated this offset using geographic information system (GIS) analysis of digitally relocated geologic features of Dibblee (1960c) onto 1-m-resolution orthophotographs to obtain a slip of 3.2 ± 0.2 km (Table 2). We applied this revised slip estimate to the entire length of the Helendale fault because of a lack of data and the absence of obvious structures that could transfer slip away or absorb slip in off-fault deformation. Due to this extrapolation, we raised the uncertainty in the error analysis for the central and northern parts of the Helendale fault. Even doubling the uncertainty for this slip value adds little to the overall uncertainty across the region. To the north, the western boundary of the central Mojave Desert is the Lockhart fault, which is discussed in the following sections.

### Slip Analysis Model of the Central Mojave Desert

We use three northeast-oriented transects to examine along-strike changes in dextral slip of the central Mojave Desert system (Fig. 7). Because most faults lack multiple estimates for offset along strike, we used a model in which slip behaves similarly to that observed on the Blackwater fault. This model applies the one or two locally derived slip values to the entire length of the regional faults, except where significant step-over structures exist, at which points lateral slip transfer was evaluated. Step-overs are recognizable in the geology, geophysics, and geomorphology of the area. The total slip for each transect was compiled using fault slip estimates or weighted means for fault segments with multiple estimates. The errors for each transect were added in quadrature to compute the slip

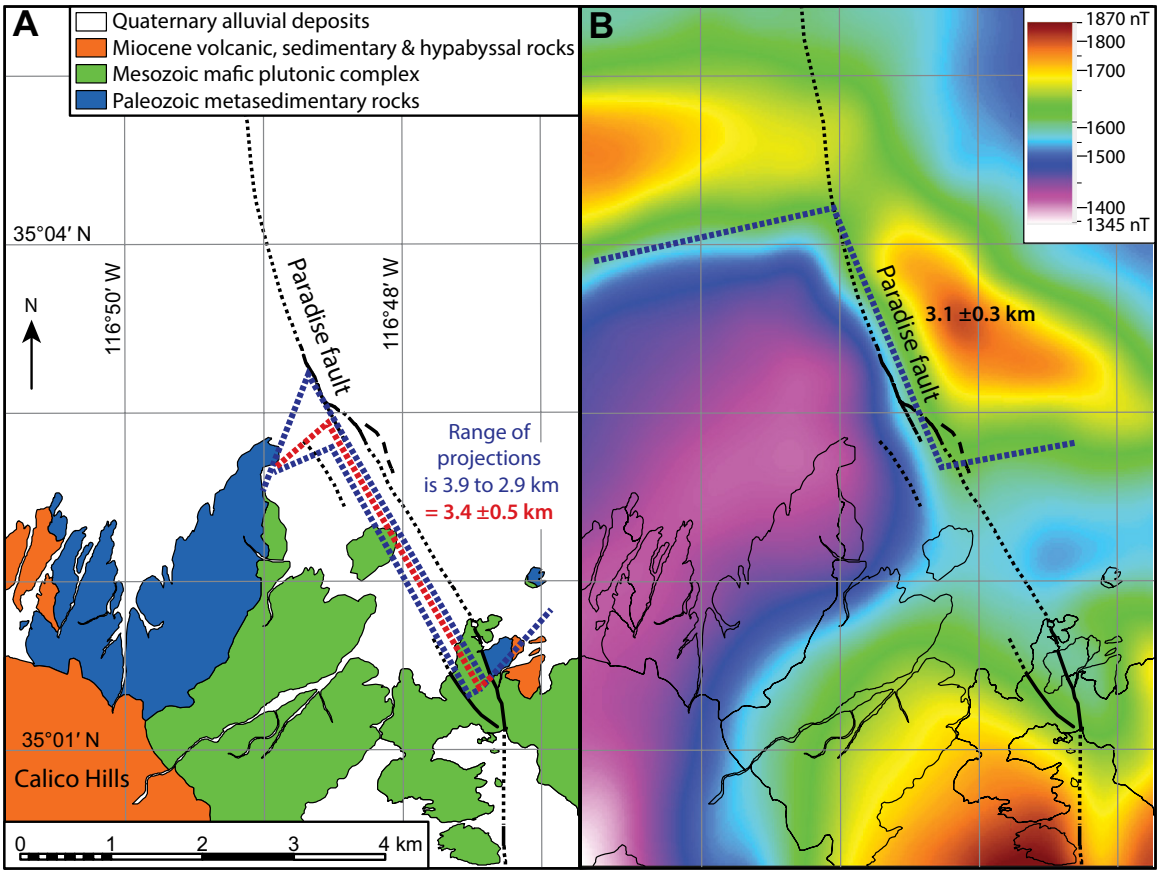


**Figure 5. (A) Simplified geologic map modified from McCulloh (1960) and Dudash (2006) showing dextral offset of Paleozoic metasedimentary rocks. See Figure 1 for location. The red dashed lines represent extremes of projection of the southern edge of the Paleozoic rocks to the Paradise fault. (B) Detailed aeromagnetic data (Jachens et al., 2002) for the same area as part A overlain by geologic map features from part A. We use the inflection of the slope of the aeromagnetic data on the southern side of the magnetic high as our reconstruction marker. These data have been adjusted to an arbitrary datum.**

uncertainty. This approach is justified in that the errors on slip estimates for different faults are random and uncorrelated. From this approach, we get estimates of slip of 14.2 ± 1.0 km for the northern, 18.1 ± 1.0 km for the central, and 17.8 ± 1.0 km for the southern transects (all quoted at 2σ).

The central and southern transects (Fig. 7) have similar amounts of offset despite differences in the locus of deformation and structural complexities. First, slip is localized on the Calico fault along the eastern side of the southern transect, and the locus of slip is farther westward on the Harper Lake fault in the central transect. This change does not seem to impact total slip. Second, slip is distributed across a wider zone in the central transect. Both the change in location and dispersion of the locus of slip appear to be accommodated by the Lenwood anticline, an east-trending transpressional fold with a kinematically linked reverse fault at depth, bounded to the east and west by dextral faults (Glazner and Bartley, 1994; Strane, 2007; Gurney, 2008; Frankel et al., 2008), and cut by the Harper Lake–Camp Rock fault (Cox and Wilshire, 1993). This anticline is an important contractional step-over between the southern and central transects, and it could transfer a portion of dextral shear leftward. The Lenwood anticline accommodates different amounts of contraction: 3.8 km in the western segment west of the Harper Lake–Camp Rock fault and 1.1 km to the east of this fault (Gurney, 2008). Offset on the Camp Rock fault decreases into the Lenwood anticline (Hawkins, 1976; Gurney, 2008), which Gurney (2008) interpreted as accommodation of dextral slip of the Camp Rock fault onto the western segment of the Lenwood anticline.

The northern transect in our analysis has a total slip value significantly less than the central and southern transects (~4 km). The potential differences in slip amounts and path are difficult to evaluate in the northern transect because, except for the Blackwater fault, the fault slips are inferred from data in the central and southern transects. Unlike the central and southern transects, the northern transect has additional areas where structures are present with poor or unknown slip estimates that are not taken into account in our analysis. Although slip on many of the faults is inferred from farther south, we do not consider this the primary limitation to understanding the amount of deformation. The most prospective locations to look for differences in slip are where there are potential step-over structures, discussed in the following.

We consider it likely that additional dextral slip is located on the Gravel Hills fault (Fig. 7), the northern continuation of the Harper Lake fault. A contractional structure similar to the Lenwood anticline exists between the northern and central transects in the termination zone of the Calico and Blackwater faults (Fig. 7). This structure begins at the Blackwater and Calico faults and trends westward and ends at

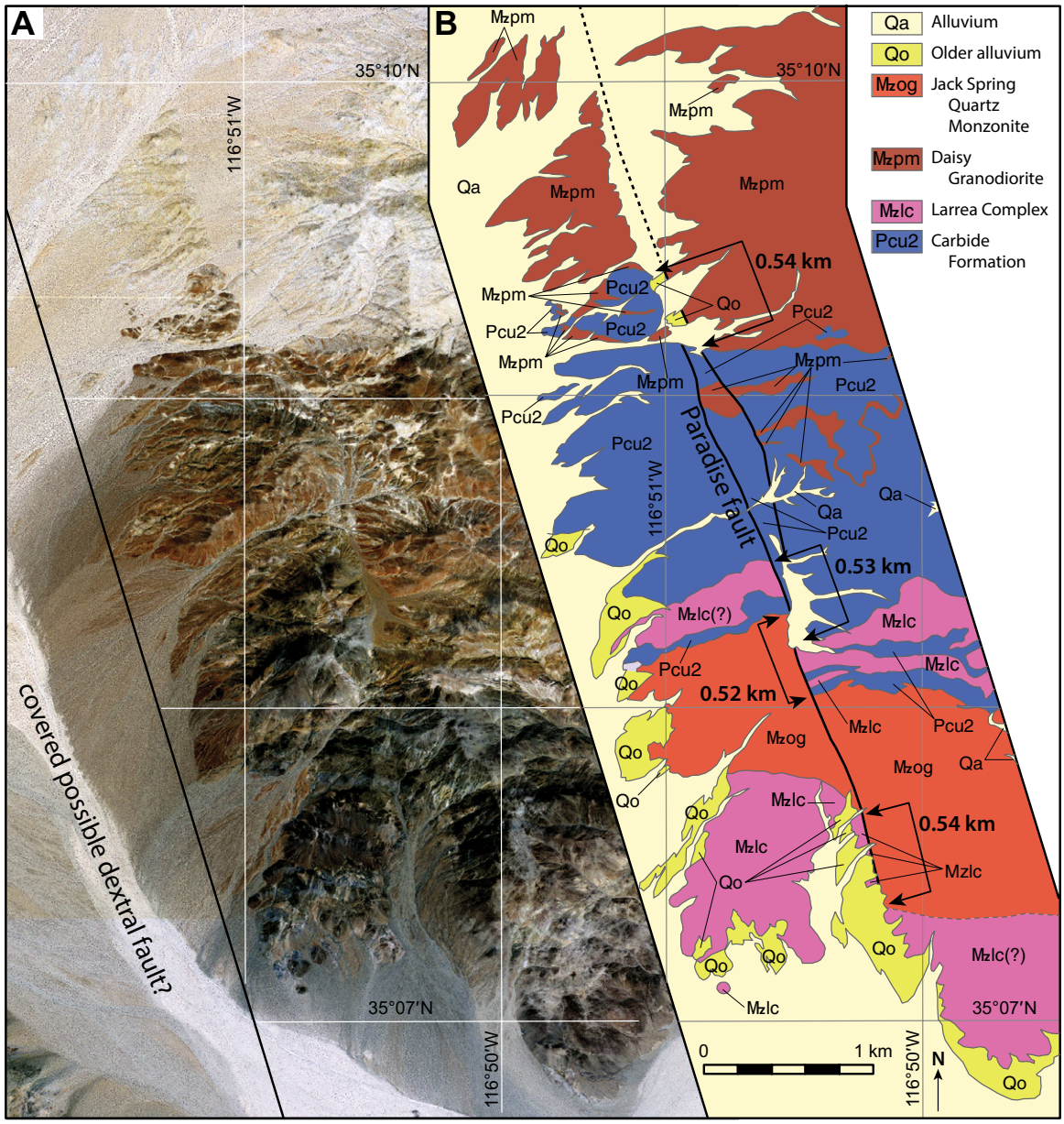


**Figure 6. (A) Detailed (1-m-resolution) orthophoto images of the Paradise Range. See Figure 1 for location. (B) Reinterpreted geologic map of McCulloh (1960) of the same area as Figure 6A showing offset of the Paradise fault. A similar amount of offset was independently interpreted by Miller et al. (2013) also using the geologic map of McCulloh (1960).**

the Gravel Hills fault (Dibblee, 1968). Pliocene basalt lava flows in this contractional zone have over 700 m of structural relief (Glazner and Bartley, 1994). This zone may act as a leftward step-over, transferring a portion of the offset of the Calico fault (and possibly the southern Paradise fault) westward onto the Gravel Hills fault, similar to our interpretation of the Lenwood anticline. This idea is partially supported by the observation that the Blackwater fault has significantly less slip (1.2 km) than the Calico fault (Fig. 7; Table 2). There are no known geologic markers along the Gravel Hills fault to test this hypothesis, but aeromagnetic patterns show an apparent dextral offset of 6–9 km along the Gravel Hills fault (for location, see Fig. 7), compared to the 4.8 km of dextral slip on the Harper Lake fault farther south. It is therefore possible that at least some (1.2 km) and perhaps all (4.2 km) of the slip difference between the northern and central/southern transects could be accommodated on the Gravel Hills fault.

Another area with large uncertainty in the northern transect is the northeastern part of the central Mojave Desert. The main issue is what happens to the slip on the Paradise fault going northward into the area of the northern transect. There are two structural scenarios for the eastern boundary, one in which the eastern boundary of the northern central Mojave Desert is the Paradise fault, and the other where the boundary steps eastward to the east Goldstone Lake fault (Fig. 7) via a segment of the Coyote Lake fault (Miller and Yount, 2002; Miller et al., 2007). If the eastern boundary of the central Mojave Desert is the Paradise fault, then there is signifi-

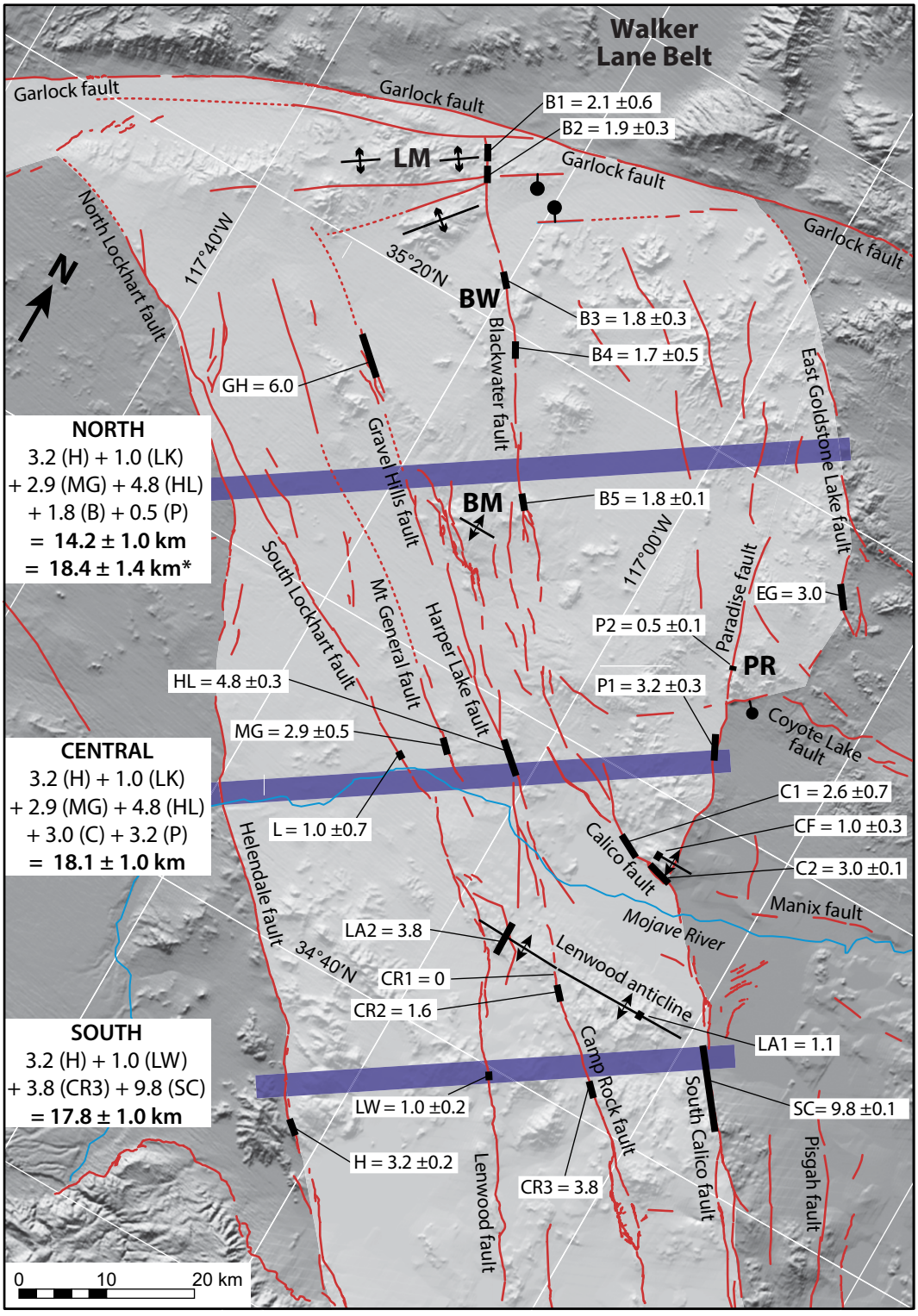


**Figure 7. Shaded relief map of the central Mojave Desert portion of the Eastern California shear zone (area highlighted in white) showing the compiled total fault slip data (details and labels on Table 2). See Figure 1 for location. The fault slip value is represented to scale by the length of the thick black line segments. The red lines are Quaternary faults modified from Amoroso and Miller (2006), Bedrossian et al. (2012), Miller et al. (2013), and Andrew et al. (2014). Mesoscopic folds with north-south contraction are shown by a double arrow symbol (Glazner and Bartley, 1994), and interpreted normal faults are shown by ball and bar symbols. Thick purple lines are transects used to examine the total slip budget of the central Mojave Desert portion of the Eastern California shear zone. Each transect is labeled and includes a summary of the individual slip values and the total slip in bold. The total slip value for the northern transect denoted with an asterisk is our preferred slip model where the Gravel Hills fault accommodates an extra 1.2 km more than the along-strike Harper Lake fault and includes the east Goldstone fault: 3.2 (H) + 1.0 (LK) + 2.9 (MG) + 6.0 (GH) + 1.8 (B) + 0.5 (P) + 3 (EG). Bold labels are Black Mountain (BM), Blackwater Well (BW), Lava Mountains (LM), and Paradise Range (PR).**

cant dextral slip that is missing or somehow absorbed in this area. A portion of the slip could be present on the poorly known faults between the Blackwater and Paradise faults (Fig. 7), but we consider large amounts of slip in this area to be unlikely because no through-going faults or significant offsets have been identified (Amoroso and Miller, 2006; Miller et al., 2013).

It is possible that slip from the Paradise fault is transferred eastward via a segment of the Coyote Lake fault (Miller et al., 2007) to the east Goldstone Lake fault (Fig. 7). Offset along the east Goldstone fault is poorly known, with possibly 3 km of dextral offset as suggested by Schermer et al. (1996) to the east of the Paradise Range (Fig. 7; Table 2). Including the east Goldstone Lake fault increases the dextral slip of the northern transect to 17.2 km, closer to the

value of the central and southern transects. This scenario would imply that the Coyote Lake fault is a right-stepping extensional step-over.

Our preferred interpretation is that a combination of these two scenarios accounts for the apparent slip difference between the northern and central transects. Dextral slip of 1.2 km from the Calico fault is transferred westward onto the Gravel Hills fault via a leftward step-over at Black Mountain, and most of the slip on the Paradise fault in the Calico Hills is transferred eastward to the east Goldstone Lake fault via a segment of the Coyote Lake fault. The total slip of the northern transect, with the interpreted 6 km of slip on the Gravel Hills fault (4.8 km from the Harper Lake fault plus 1.2 km from the Calico fault) and including the slip of the east Goldstone Lake fault, is 18.4 ± 1.4 km of slip (Fig. 7), which agrees closely with the total slip of central and southern transects.

### Summary of Regional Slip and Slip Initiation

Previous studies interpreted the difference between 9.8 km of slip on the southern portion of the Calico fault and 1.8 km of slip on the southern Blackwater fault as gradually decreasing amounts of slip northward in the central Mojave Desert portion of the Eastern California shear zone. Our results lead us to a different interpretation of the regional fault system. First, the overall amount of slip is consistent from south to north in the central Mojave Desert portion of the Eastern California shear zone. Second, significant changes in the amounts of total fault offset on individual faults occur via transverse structures that laterally link the dextral faults to allow transfer of slip from one fault to another. Our analysis is limited by the lack of detailed information for the northern portions of the Lockhart, Helendale, Mount General, and Harper Lake (segment referred to as the Gravel Hills fault) faults and the poorly constrained east Goldstone Lake fault.

We interpret dextral slip on the Blackwater fault to have begun at or after ca. 3.8 Ma. This Pliocene age of initiation may apply to other parts of the central Mojave Desert, but there are few known constraints. The Lenwood fault is interpreted to be younger than an offset 7.33 Ma lava flow (unpublished Ar-Ar data from A. Iriondo *cited in* Frankel et al., 2008). Dextral faulting in the western parts of the central Mojave Desert (Helendale fault) was interpreted by Cox et al. (2003) to have begun at 1.5 Ma based on stratigraphic data and evolution of the Mojave River. The modern fault-controlled physiography of the northeastern Mojave Desert, northeast of the central Mojave Desert (Fig. 1), began after 3.4 Ma (Miller and Yount, 2002). Although the initiation of faulting in the northeastern Mojave Desert was constrained by Schermer et al. (1996) to have occurred after 11 Ma rocks, Miller and Yount (2002) interpreted the data of Schermer et al. (1996) to state that a few of the faults in the northeastern Mojave Desert have similarly displaced 17 Ma and 5.6 Ma rocks, implying a Pliocene or younger age of fault initiation. A Pliocene age of initiation fits with calculated initiation times for the central Mojave Desert of 2–4 Ma (Du and Aydin, 1996) and ca. 3.4 Ma (Gan et al., 2003) using neotectonic and geodetic data. Dokka and Travis (1990) speculated that the initiation of dextral slip in the Eastern California shear zone may have progressed westward with time, but the limited available data do not preclude either instantaneous or progressive development of faults. To the north in the along-strike Walker Lane belt, initiation of dextral slip initiated progressively westward and overlaps in time with timing constraints for the central Mojave Desert (Burchfiel et al., 1987; Monastero et al., 2002; Mahéo et al., 2009; Andrew and Walker, 2009; Walker et al., 2014).

## CONCLUSIONS

Geologic slip estimates for the Blackwater fault are consistent at ~1.8 km of dextral slip along 55 km of strike length and are inconsistent with previous hypotheses of decreasing slip northward. Existing data combined with regional new total offset estimates show consistent amounts of total dextral slip on the faults in the southern and central Mojave Desert. We use this interpretation of consistent slip to pose a hypothesis for the central Mojave Desert fault system that dextral slip is constant from south to north. The strain path changes along strike, and the locus of dextral slip steps westward and is more diffuse from south to north. Along-strike changes in the central Mojave Desert fault system are accommodated by contractional and extensional step-overs that laterally transfer strain. The total dextral slip across the central Mojave Desert is ~18 km (averaged value for the southern and central transects on Fig. 7). The locus of the greatest amount of slip in the south is on the Calico fault, and this dextral slip steps westward northward onto the Harper Lake fault in the central transect area and northward onto the Gravel Hills fault in the northern transect. The northern central Mojave Desert, however, is problematic, because it is more complex and has fewer available fault slip data, with the exception of the now well-known Blackwater fault.

We interpret the central Mojave Desert as part of a through-going zone of dextral stain all the way to and across the Garlock fault, in agreement with geodetic data (Peltzer et al., 2001). The faults of the central Mojave Desert do not cut the Garlock fault, which apparently acts as a barrier. A similar amount of dextral slip occurs to the north of the Garlock fault in the Walker Lane belt (Monastero et al., 2002; Walker et al., 2005; Andrew and Walker, 2009). The 18 km of dextral strain across the Garlock fault must be accommodated via other processes: bending, complex faulting, folding, and vertical axis rotation, as well as localized steps developed along the Garlock fault (Andrew et al., 2014). We interpret the through-going fault slip barrier behavior of the Garlock fault to cause the Eastern California shear zone in the central Mojave Desert to become wider and more diffuse as it approaches the Garlock fault (compare the concentration of over 50% of the fault slip in the southern transect on one fault [Calico fault] with the wider zone of faulting in the northern transect, in which there are more faults with the largest offset fault [Gravel Hills fault] only accommodating a third of the total slip; Fig. 7). This is very similar in scale and structural configuration to the behavior of the dextral Xianshuihe-Xiaojiang fault as it intersects the through-going, sinistral Red River fault zone in southern China (Schoenbohm et al., 2006).

#### ACKNOWLEDGMENTS

This work was partly supported by a grant from the Geothermal Program Office of the U.S. Department of the Navy, China Lake, and by the EarthScope Program of the National Science Foundation. We wish to thank Frank Monastero, Andy Sabin, and Tandis Bidgoli for discussions on Mojave strike-slip faulting. Bidgoli also provided a very helpful review of an earlier version of this manuscript. Michael Oskin, a *GSA Bulletin* associate editor, and an anonymous reviewer made suggestions for improvement of an earlier version of this paper. Significant improvements resulted from reviews by Gilles Peltzer, David Miller, and David Schofield.

#### REFERENCES CITED

Amoroso, L., and Miller, D.M., 2006, Surficial Geologic Map of the Cuddeback Lake 30′ × 60′ Quadrangle, San Bernardino and Kern Counties, California: U.S. Geological Survey Open-File Report 2006-1276, scale 1:100,000, 31 p.

Andrew, J.E., and Walker, J.D., 2009, Reconstructing late Cenozoic deformation in central Panamint Valley, California: Evolution of slip partitioning in the Walker Lane: Geosphere, v. 5, p. 172–198, doi:10.1130/GES00178.1.

Andrew, J.E., Walker, J.D., and Monastero, F.C., 2014, Evolution of the central Garlock fault zone, California: A major sinistral fault embedded in a dextral plate margin: Geological Society of America Bulletin, v. 127, p. 227–249, doi:10.1130/B31027.1.

Bartley, J.M., Glazner, A.F., and Schermer, E.R., 1990, North-south contraction of the Mojave block and strike-slip tectonics in southern California: Science, v. 248, p. 1398–1401, doi:10.1126/science.248.4961.1398.

Bartley, J.M., Glazner, A.F., Fletcher, J.M., Martin, M.W., and Walker, J.D., 1992, Amount and nature of dextral offset on Neogene faults near Barstow, California: Eos, Transactions of the American Geophysical Union, v. 73, Fall meeting supplement, p. 363.

Bedrossian, T.L., Roffers, P., Hayhurst, C.A., Lancaster, J.T., and Short, W.R., 2012, Geologic Compilation of Quaternary Surficial Deposits in Southern California: Department of Conservation, California Geological Survey Special Report 217, 21 p.

Bird, P., 2009, Long-term fault slip rates, distributed deformation rates, and forecast of seismicity in the western United States from joint fitting of community geologic, geodetic, and stress direction data sets: Journal of Geophysical Research, v. 114, B11403, doi:10.1029/2009JB006317.

Boettcher, S.S., 1990, Geologic Map of Iron Mountain: Geological Society of America Digital Map and Chart Series 19, 1:12,000 scale, doi:10.1130/1990-boettcher-ironmountain.

Boettcher, S.S., and Walker, J.D., 1993, Geologic evolution of Iron Mountain, central Mojave Desert, California: Tectonics, v. 12, p. 372–386, doi:10.1029/92TC02423.

Burchfiel, B.C., Hodges, K.V., and Royden, L.H., 1987, Geology of Panamint Valley–Saline Valley pull-apart system, California: Palinspastic evidence for low-angle geometry of a Neogene range-bounding fault: Journal of Geophysical Research, v. 92, p. 10,422–10,426, doi:10.1029/JB092iB10p10422.

Carleton, C.F., 1988, Tectonic Significance of Late Miocene Deposits in the Southern Fry Mountains, Mojave Desert, California [M.S. Thesis]: Riverside, California, University of California, 130 p.

Cox, B.F., and Wilshire, H.G., 1993, Geologic Map of the Area around the Nebo Annex, Marine Corps Logistics Base, Barstow, California: U.S. Geological Survey Open-File Report 93-568, 36 p., scale 1:12,000.

Cox, B.F., Hillhouse, J.W., and Owen, L.A., 2003, Pliocene and Pleistocene evolution of the Mojave River, and associated tectonic development of the Transverse Ranges and Mojave Desert, based on borehole stratigraphy studies and mapping of landforms and sediments near Victorville, California, *in* Enzel, Y., Wells, S.G., and Lancaster, N., eds., Paleoenvironments and Paleohydrology of the Mojave and Southern Great Basin Deserts: Geological Society of America Special Paper 368, p. 1–42, doi:10.1130/0-8137-2368-X.1.

Dibblee, T.W., 1960a, Geologic Map of the Barstow Quadrangle, San Bernardino County, California: U.S. Geological Survey Mineral Investigations Field Studies Map MF-233, scale 1:62,500.

Dibblee, T.W., 1960b, Geologic Map of the Hawes Quadrangle, San Bernardino County, California: U.S. Geological Survey Mineral Investigations Field Studies Map MF-226, scale 1:62,500.

Dibblee, T.W., 1960c, Preliminary Geologic Map of the Apple Valley Quadrangle, California: U.S. Geological Survey Mineral Investigations Field Studies Map MF-232, scale 1:62,500.

Dibblee, T.W., 1967, Areal Geology of the Western Mojave Desert, California: U.S. Geological Survey Professional Paper 522, 153 p.

Dibblee, T.W., 1968, Geology of the Fremont Peak and Opal Mountain Quadrangles, California; California Division of Mines and Geology Bulletin 188, scale 1:62,500.

Dixon, T.H., Robaudo, S., Lee, J., and Reheis, M.C., 1995, Constraints on present-day Basin and Range deformation from space geodesy: Tectonics, v. 14, p. 755–772, doi:10.1029/95TC00931.

Dokka, R.K., and Travis, C.J., 1990, Late Cenozoic strike-slip faulting in the Mojave Desert California: Tectonics, v. 9, p. 311–340, doi:10.1029/TC009i002p00311.

Du, Y., and Aydin, A., 1996, Is the San Andreas big bend responsible for the Landers earthquake and the Eastern California shear zone?: Geology, v. 24, p. 219–222, doi:10.1130/0091-7613(1996)024<0219:ITSABB>2.3.CO;2.

Dudash, S.L., 2006, Preliminary Surficial Geologic Map of a Calico Mountains Piedmont and Part of Coyote Lake, Mojave Desert, San Bernardino County, California: U.S. Geological Survey Open-File Report 2006-1090, 48 p.

Fletcher, D.I., 1986, Geology and Genesis of the Waterloo and Langtry Silver-Barite Deposits, California [Ph.D. thesis]: Stanford, California, Stanford University, 158 p.

Fletcher, J.M., 1999, Geologic Map of the Mitchel Range and Waterman Hills: Geological Society of America Digital Map and Chart Series, scale 1:12,000, doi:10.1130/1999-fletcher-watermanhills, http://www.geosociety.org/maps/1999-fletcher-watermanhills/ (last accessed March 2017).

Fletcher, J.M., and Martin, M.W., 1998, Geologic Map of the Hinkley Hills: Geological Society of America Digital Map and Chart Series, scale 1:12,000, doi:10.1130/1998-fletcher-hinkleyhills, http://www.geosociety.org/maps/1998-fletcher-hinkleyhills/ (last accessed March 2017).

Fletcher, J.M., Bartley, J.M., Martin, M.W., Glazner, A.F., and Walker, J.D., 1995, Large-magnitude continental extension; an example from the central Mojave metamorphic core complex: Geological Society of America Bulletin, v. 107, no. 12, p. 1468–1483, doi:10.1130/0016-7606(1995)107<1468:LMCEAE>2.3.CO;2.

Frankel, K.L., Glazner, A.F., Kirby, E., Monastero, F.C., Strane, M.D., Oskin, M.E., Unruh, J.R., Walker, J.D., Anandakrishnan, S., Bartley, J.M., Coleman, D.S., Dolan, J.F., Finkel, R.C., Greene, D., Kylander-Clark, A., Morrero, S., Owen, L.A., and Phillips, F., 2008, Active tectonics of the Eastern California shear zone, *in* Duebendorfer, E.M., and Smith, E.I., eds., Field Guide to Plutons, Volcanoes, Faults, Reefs, Dinosaurs, and Possible Glaciation in Selected Areas of Arizona, California, and Nevada: Geological Society of America Field Guide 11, p. 43–81, doi:10.1130/2008.fld011(03).

Gan, W., Zhang, P., Shen, Z., Prescott, W.H., and Svarc, J.L., 2003, Initiation of deformation of the Eastern California shear zone: Constraints from Garlock fault geometry and GPS observations: Geophysical Research Letters, v. 30, 1496, doi:10.1029/2003GL017090.

Garfunkel, Z., 1974, Model for late Cenozoic tectonic history of the Mojave Desert, California, and for its relation to adjacent regions: Geological Society of America Bulletin, v. 85, p. 1931–1944, doi:10.1130/0016-7606(1974)85<1931:MFTLCT>2.0.CO;2.

Glazner, A.F., and Bartley, J.M., 1994, Eruption of alkali basalts during crustal shortening in southern California: Tectonics, v. 13, no. 2, p. 493–498, doi:10.1029/93TC03491.

Glazner, A.F., Walker, J.D., Bartley, J.M., Fletcher, J.M., Martin, M.W., Schermer, E.R., Boettcher, S.S., Miller, J.S., Fillmore, R.P., and Linn, J.K., 1994, Reconstruction of the Mojave block, *in* McGill, S.F., and Ross, T.M., eds., Geological Investigations of an Active Margin: Geological Society of America Cordilleran Section Guidebook: Redlands, California, San Bernardino County Museum Association, p. 3–30.

Glazner, A.F., Bartley, J.M., and Sanner, W.K., 2000, Nature of the southwestern boundary of the central Mojave Tertiary province, Rodman Mountains, California: Geological Society of America Bulletin, v. 112, no. 1, p. 34–44, doi:10.1130/0016-7606(2000)112<34:NOTSBO>2.0.CO;2.

Glazner, A.F., Walker, J.D., Bartley, J.M., and Fletcher, J.M., 2002, Cenozoic evolution of the Mojave block of southern California, *in* Glazner, A.F., Walker, J.D., and Bartley, J.M., eds., Geologic Evolution of the Mojave Desert and Southwestern Basin and Range: Geological Society of America Memoir 195, p. 19–41, doi:10.1130/0-8137-1195-9.19.

Gurney, E., 2008, Camp Rock Fault Slip Rate and Folding of the Lenwood Anticline: Contributions to Eastern California Shear Zone Strain Accumulation [M.S. thesis]: Chapel Hill, North Carolina, University of North Carolina, 53 p.

Hawkins, H.G., 1976, Strike Slip Displacement along the Camp Rock Fault, Central Mojave Desert, San Bernardino, California [M.S. thesis]: Los Angeles, University of Southern California, 63 p.

Jachens, R.C., Langenheim, V.E., and Matti, J.C., 2002, Relationship of the 1999 Hector Mine and 1992 Landers fault ruptures to offsets on Neogene faults and distribution of late Cenozoic basins in the Eastern California shear zone: Bulletin of the Seismological Society of America, v. 92, p. 1592–1605, doi:10.1785/0120000915.

Jenkins, S.L., 1989, Geology, alteration and mineralization of the Blackwater hydrothermal cell; San Bernardino County, California, *in* The California Desert Mineral Symposium (Compendium): California State Office, South Coast Geological Society, U.S. Department of the Interior Bureau of Land Management, p. 177–193.

Mahéo, G., Saleeby, J., Saleeby, Z., and Farley, K.A., 2009, Tectonic control on southern Sierra Nevada topography, California: Tectonics, v. 28, TC6006, doi:10.1029/2008TC002340.

McCulloh, T.H., 1960, Geologic Map of the Lane Mountain Quadrangle, California: U.S. Geological Survey Open-File Report OF-60-95, scale 1:48,000.

Meade, B.J., and Hager, B.H., 2004, Block models of present crustal motion in southern California constrained by GPS measurements: Journal of Geophysical Research, v. 110, B03403, doi:10.1029/2004JB003209.

Miller, F.K., and Morton, D.M., 1980, Potassium-Argon Geochronology of the Eastern Transverse Ranges and Southern Mojave Desert, California: U.S. Geological Survey Professional Paper 1151, 30 p.

Miller, D.M., and Yount, J.C., 2002, Late Cenozoic evolution of the north-central Mojave Desert inferred from fault history and physiographic evolution of the Fort Irwin area, California, *in* Glazner, A.F., Walker, J.D., and Bartley, J.M., eds., Geologic Evolution of the Mojave Desert and Southwestern Basin and Range: Geological Society of America Memoir 195, p. 173–197, doi:10.1130/0-8137-1195-9.173.

Miller, D.M., Dudash, S.L., Green, H.L., Lidke, D.J., Amoroso, L., Phelps, G.A., and Schmidt, K.M., 2007, A new Quaternary view of northern Mojave Desert tectonics suggests changing fault patterns during the late Pleistocene, *in* Miller, D.M., and Valin, Z.C., eds., Geomorphology and Tectonics at the Intersection of Silurian and Death Valleys, Southern California: U.S. Geological Survey Open-File Report 2007-1424, p. 157–171.

Miller, D.M., Menges, C.M., and Lidke, D.J., 2013, Generalized Surficial Geologic Map of the Fort Irwin Area, San Bernardino County, California: U.S. Geological Survey Open-File Report 20131024-B, scale 1:100,000, 11 p., doi:10.3133/ofr20131024B.

Miller, M.M., Johnson, D.J., Dixon, T.H., and Dokka, R.K., 2001, Refined kinematics of the Eastern California shear zone from GPS observations, 1993–1998: Journal of Geophysical Research, v. 106, p. 2245–2263, doi:10.1029/2000JB900328.

Monastero, F.C., Walker, J.D., Katzenstein, A.M., and Sabin, A.E., 2002, Neogene evolution of the Indian Wells Valley, east-central California, *in* Glazner, A.F., Walker, J.D., and Bartley, J.M., eds., Geologic Evolution of the Mojave Desert and Southwestern Basin and Range: Geological Society of America Memoir 195, p. 199–228, doi:10.1130/0-8137-1195-9.199.

Oskin, M., and Iriondo, A., 2004, Large-magnitude transient strain accumulation on the Blackwater fault, Eastern California shear zone: Geology, v. 32, p. 313–316, doi:10.1130/G20223.1.

Oskin, M., Perg, L., Blumentritt, D., Mukhopadhyay, S., and Iriondo, A., 2007, Slip rate of the Calico fault: Implications for geologic versus geodetic rate discrepancy in the Eastern California shear zone: Journal of Geophysical Research, v. 112, B03402, doi:10.1029/2006JB004451, 16 p.

Peltzer, G., Crampe, F., Hensley, S., and Rosen, P., 2001, Transient strain accumulation and fault interaction in the Eastern California shear zone: Geology, v. 29, p. 975–978, doi:10.1130/0091-7613(2001)029<0975:TSAAFI>2.0.CO;2.

Plesch, A., Shaw, J.H., Bryant, W.A., Carena, S., Cooke, M.L., Dolan, J.F., Fuis, G.S., Gath, E.M., Grant Ludwig, L.B., Hauksson, E., Jordan, T.H., Kamerling, M.J., Legg, M.R., Lindvall, S.C., Magistrale, H., Nicholson, C., Niemi, N.A., Oskin, M.E., Perry, S.C., Planansky, G., Rockwell, T.K., Shearer, P.M., Sorlien, C.C., Suess, M., Suppe, J., Treiman, J.A., and Yeats, R.S., 2007, Community fault model (CFM) for southern California: Bulletin of the Seismological Society of America, v. 97, p. 1793–1802, doi:10.1785/0120050211.

Schermer, E., Luyendyk, B.P., and Cisowski, S., 1996, Late Cenozoic structure and tectonics of the northern Mojave Desert: Tectonics, v. 15, p. 905–932, doi:10.1029/96TC00131.

Schoenbohm, L.M., Burchfiel, B.C., Liangzhong, and Jiyun, Y., 2006, Miocene to present activity along the Red River fault, China, in the context of continental extrusion, upper-crustal rotation, and lower-crustal flow: Geological Society of America Bulletin, v. 118, p. 672–688, doi:10.1130/B25816.1.

Singleton, J.S., and Gans, P.B., 2008, Structural and stratigraphic evolution of the Calico Mountains: Implications for early Miocene extension and Neogene transpression in the central Mojave Desert, California: Geosphere, v. 4, no. 3, p. 459–479, doi:10.1130/GES00143.1.

Smith, G.I., 1964, Geology and Volcanic Petrology of the Lava Mountains, San Bernardino County, California: U.S. Geological Survey Professional Paper 457, 97 p.

Stewart, J.H., 1988, Tectonics of the Walker Lane belt, western Great Basin: Mesozoic and Cenozoic deformation in a shear zone, *in* Ernst, W.G., ed., Metamorphism and Crustal Evolution of the Western United States: Englewood Cliffs, New Jersey, Prentice-Hall, p. 681–713.

Strane, M.D., 2007, Slip Rate and Structure of the Nascent Lenwood Fault Zone, Eastern California [M.S. thesis]: Chapel Hill, North Carolina, University of North Carolina, 65 p.

Walker, J.D., Bartley, J.M., and Glazner, A.F., 1990, Large magnitude Miocene extension in the central Mojave Desert: Implications for Paleozoic to Tertiary paleogeography and tectonics: Journal of Geophysical Research, v. 95, p. 557–569, doi:10.1029/JB095iB01p00557.

Walker, J.D., Fletcher, J.M., Fillmore, R.P., Martin, M.W., Taylor, W.J., Glazner, A.F., and Bartley, J.M., 1995, Connection between igneous activity and extension in the central Mojave metamorphic core complex, California: Journal of Geophysical Research, v. 100, p. 10,477–10,494, doi:10.1029/94JB03132.

Walker, J.D., Black, R.A., Berry, A.K., Davis, P.J., Andrew, J.E., and Mitsdarfer, J.M., 2002, Geologic maps of the northern Mojave Desert and southwestern Basin and Range Province, *in* Glazner, A.F., Walker, J.D., and Bartley, J.M., eds., Geologic Evolution of the Mojave Desert and Southwestern Basin and Range: Geological Society of America Memoir 195, p. 295–296, scale 1:250,000.

Walker, J.D., Andrew, J.E., and Kirby, E., 2005, Strain transfer and partitioning between the Panamint Valley, Searles Valley, and Ash Hill fault zones, California: Geosphere, v. 1, no. 3, p. 111–118, doi:10.1130/GES00014.1.

Walker, J.D., Bidgoli, T.S., Diderickson, B.D., Stockli, D.F., and Andrew, J.F., 2014, Middle Miocene to recent exhumation of the Slate Range, eastern California, and implications for the timing of extension and the transition to transtension: Geosphere, v. 10, p. 276–291, doi:10.1130/GES00947.1.

Science Editor: David I. Schofield
Associate Editor: Nancy Riggs

Manuscript Received 7 March 2016
Revised Manuscript Received 29 September 2016
Manuscript Accepted 15 February 2017

Printed in the USA